

Large Chern-Number Quantum Anomalous Hall Effect from Canted Antiferromagnetic Order in d -Electron System on Kagome Lattice

Waquar Ahmed,¹ Steffen Schäfer,¹ Pierre Lombardo,¹ Roland Hayn,¹ and Imam Makhfudz¹
 IM2NP, UMR CNRS 7334, Aix-Marseille Université, 13013 Marseille, France

(Dated: 16 September 2025)

Electrons of d -symmetry in a kagome lattice are considered which interact with non-collinear antiferromagnetic order in the absence of spin-orbit coupling. The non-collinearity of spin texture gives rise to non-relativistic spin splitting and the associated intrinsic Berry curvature. The integral of the latter over the Brillouin zone becomes nontrivial for non-coplanar (canted) non-collinear spin order even without explicit on-site or transfer spin-orbit coupling. That gives rise to a nonzero (scalar) spin chirality, and a record value for the Chern number of $C = \pm 5$ can appear when the Fermi level is in an appropriate gap for isotropic electron hopping integrals, or nearly isotropic ones. The numerical results for this topological quantum anomalous Hall effect are supported by an analytical formula. It is possible to split the $C = \pm 5$ plateau into different possible nonzero values for the Chern number by varying the onsite energies. The topological phase transitions between Hall plateaus can be driven by flipping the Zeeman-like exchange field or controlling the onsite energies, alluding to the potential of this system to quantum information.

Introduction.—Anomalous Hall effect (AHE), where an electric current produces a transverse voltage due to time-reversal symmetry breaking without external magnetic field, has been at the forefront of condensed matter physics research, due to its potential applications in dissipation-less electronics¹.

Millennial-era advance in condensed matter physics research is marked with the discovery of materials with electronic structures hosting peculiar features such as Dirac points and flatbands^{2–4}. When magnetism is present in such materials, one can have either frustration-induced quantum spin liquid state^{6,7}, or magnetically ordered state which may give rise to AHE. While AHE can be driven by extrinsic mechanisms induced by impurity or disorder, a more fundamental perspective supposes that AHE can occur in clean system, relying on the internal spin order or processes within the materials. Indeed, AHE induced by non-collinear or chiral spin order^{8–15,18,19} or by the effective magnetic field in reciprocal space (Berry curvature)^{20,21,22} have been postulated. The latter mechanism gives rise to the quantum anomalous Hall effect (QAHE)²³ characterized by an integer -the Chern number^{24,1}, as proposed to occur in diverse systems^{25,26,27,28,29,30,31} with experimental verification^{32,33}. A recent work of us demonstrates the occurrence of QAHE in d -electron system on kagome lattice with ferromagnetic order³⁴.

A key ingredient of AHE and QAHE is time-reversal symmetry breaking. The latter is guaranteed in ferromagnets by the ferromagnetic ordering with net magnetization. In antiferromagnets on the other hand, net magnetization is zero, making the order uncontrollable with external magnetic field. This has led to the conventional belief that antiferromagnets are not useful for applications, a view that has been challenged by recent developments, which demonstrate that antiferromagnets may nevertheless host interesting effects that can be useful for applications, leading to the new research area of antiferromagnetic spintronics³⁵. It is well understood that in collinear bipartite antiferromagnets, as applicable to honeycomb lattice antiferromagnets, where spins are ordered with staggered antiparallel configuration, the net magnetization is zero and the electronic structure

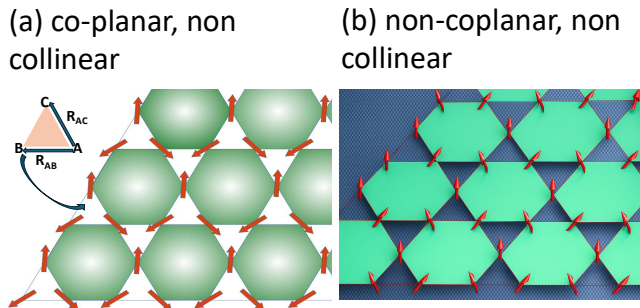


FIG. 1. (a) Coplanar noncollinear spin order with three sublattices, each carrying a spin at 120° from each other. (b) An artistic 3D side view of a non-coplanar version obtained by adding an out of plane component to the spin orientation. Different spin configurations with the same unit cell related by permutation of the three sublattices' spin vectors are degenerate in spin energy.

is two-fold degenerate in spin. A less obvious situation is when the spins are ordered non-collinearly but with zero net magnetization, leading to the so-called non-collinear antiferromagnetic order, as pertinent in triangular and kagome lattices³⁶. Non-quantized AHE has been suggested theoretically from non-collinear antiferromagnetic order involving spin-orbit coupling on kagome lattice¹⁵ and observed experimentally, with large anomalous Hall conductivity^{16,17}. Canted ferromagnet and antiferromagnetic orders near collinearity with spin chirality, have been predicted theoretically to give rise to chiral Hall effect³⁷ and demonstrated experimentally from non-coplanar spin order in van der Waals materials³⁸. QAHE in s -orbital conduction electron system due to canted spin order of localized d -orbital electrons has been studied³⁹, while in transition-based compounds, the physics is dominated by d -orbital (instead of s) conduction electrons, leaving open the problem on the fate of QAHE in such multi-orbital system.

A natural question is therefore whether QAHE can occur in a multi-orbital d -electron system with non-collinear spin

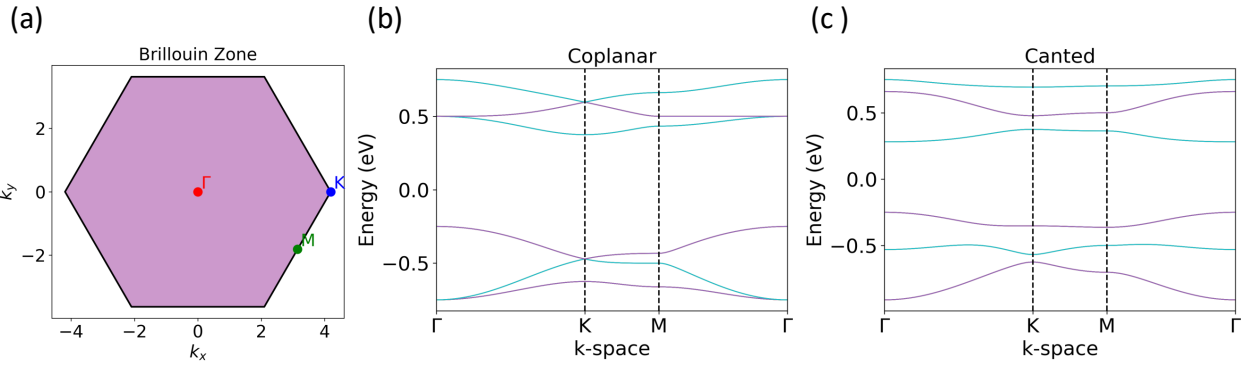


FIG. 2. Band structures of d -orbital electrons along the $K - \Gamma - M - \Gamma$ path in the first Brillouin zone (a) for the kagome model Eq.(1) with (b)co-planar collinear spin order (c)non-coplanar spin order, for the isotropic Slater-Koster integrals. Both band structures demonstrate spin-splitting due to the non-collinear spin order; (b)large trivial gap and (c)large trivial gap and small nontrivial gaps. To produce Fig. 2(b) and (c), we have used $E_1 = E_2 = E_3 = 0.0\text{eV}$, $V_{dd\pi} = V_{dd\delta} = V_{dd\sigma} = -0.25\text{eV}$, and representing the moment as $\mathbf{M}(\mathbf{r}) = (M_x(\mathbf{r}), M_y(\mathbf{r}), M_z(\mathbf{r})) = M_s(\sin \theta_{\mathbf{r}} \cos \phi_{\mathbf{r}}, \sin \theta_{\mathbf{r}} \sin \phi_{\mathbf{r}}, \cos \theta_{\mathbf{r}})$, $M_s = 1.0\text{eV}$ with polar angle (b) $\theta_{\mathbf{r}} = 90^\circ$ and (c) $\theta_{\mathbf{r}} = 53^\circ$, while the azimuthal angle $\phi_{\mathbf{r}}$ takes the 120° configuration of the three sublattices A, B, and C in Fig. 1(a).

order but *without* spin-orbit coupling (SOC). The orbital degree of freedom can either disrupt or reinforce the QAHE. The spins are coupled to the conduction electron and may induce a spin-dependent effective flux in real space, giving a complex hopping integral for the electron and spin-splitting in electronic structure, despite zero net magnetization. Coplanar collinear spin order turns out to give no quantum anomalous Hall effect due to trivial real space flux, even with anisotropic hopping integral, unless one introduces a transfer-type spin-orbit coupling¹⁵. The topological quantum anomalous Hall effect requires non-coplanar non-collinear spin order and we report here on the manifestation of the quantum version of the topological Hall effect in multi-orbital system.

All the five orbitals contribute to nonzero Chern number, with opposite signs for the two spin sectors which, under certain conditions, give a record-breaking Chern number $C = \pm 5$, which would be the largest Chern number known to date to occur in natural quantum materials without heterostructure engineering.

Model — A minimal tight-binding model is considered, consisting of hopping term for d -electrons and its coupling to Zeeman-like exchange field from the spin order, plus onsite energy term that lifts the degeneracy between different d -orbitals :

$$H = \frac{1}{2} \sum_{\langle ij \rangle} t_{ij,\alpha\alpha'} d_{i,\alpha\sigma}^\dagger d_{j,\alpha'\sigma} + \text{h.c.} + \sum_i E_\alpha d_{i,\alpha\sigma}^\dagger d_{i,\alpha\sigma} - \sum_{i,\alpha\sigma'} d_{i,\alpha\sigma}^\dagger (\mathbf{M}_i \cdot \mathbf{s})_{\sigma,\sigma'} d_{i,\alpha\sigma'} \quad (1)$$

$d_{i,\alpha\sigma}^\dagger (d_{i,\alpha\sigma})$ are creation (annihilation) operators for d -electrons of spin σ in orbital α and on site i (Fig.1), and the hopping matrix elements $t_{ij,\alpha\alpha'}$ in the first term are linear functions of Slater-Koster integrals $V_{dd(\sigma/\pi/\delta)}$ for hopping of electrons between two d orbitals⁴⁰. The second term accounts for the onsite energies are in general different for

the five d -orbitals⁴¹, but in simpler case is assumed to be degenerate with three different values: E_1 for the d_{z^2} -orbital, E_2 for the d_{xz} and d_{yz} -orbital, and E_3 for d_{xy} and $d_{x^2-y^2}$. The third term represents the “Zeeman term” giving a spin splitting due to a exchange field induced by the non-collinear spin order, corresponding to sublattice-dependent magnetic moment \mathbf{M}_i , $i \in A, B, C$, the planar projection of which forms 120° with respect to each other as illustrated in Fig. 1, giving zero net magnetization when coplanar on the plane ($M_z = 0$). When M_z is also nonzero, one obtains non-coplanar canted spin order. As to be seen later, the non-collinear magnetic structure gives rise to non-relativistic spin splitting.

Band Structure: Non-relativistic spin splitting.—The first step in going from the model Hamiltonian Eq.(1) is to compute the band structure, done in the basis of the electron state (5 orbitals times 3 sublattices times 2 spin states). The Hamiltonian is written in \mathbf{k} space via Fourier transform with periodic boundary condition. The unit vectors in real lattice space are shown in Fig. 1.

Presented in Fig.2 are the band structures in the presence of non-collinear spin order, with coplanar and non-coplanar configurations. The parameters for kinetic hopping term have been chosen to have the highest symmetry and give the simplest profile of band structure, with flatband and quadratic and linear (Dirac) crossing points⁴²; $V_{dd\sigma} = V_{dd\delta} = V_{dd\pi}$ for the Slater-Koster integrals. This ‘isotropic limit’ is a special case; real materials normally have anisotropic Slater-Koster integrals. It will be shown here that the isotropic limit serves as a good starting reference point from which the physics of real materials can be described by adding anisotropy.

As can be seen from Fig. 2(b), the coplanar non-collinear spin order splits the spin up bands and spin down bands from each other. This marks the distinction between coplanar non-collinear spin order in frustrated geometry like kagome lattice and collinear antiferromagnetic order in bipartite lattice; despite vanishing net magnetization in both cases, in the latter, there is no spin-splitting, i.e., the bands are two-fold spin degenerate. The coplanar non-collinear spin order lifts the

Kramers degeneracy, even though the net magnetization is zero.

Considering canted spin order gives rise to a very neat band structure with big trivial gap and significant non-trivial gaps $\delta E \sim 100$ to 150meV for $M_s = 1.0\text{eV}$ at the same time, as illustrated in Fig. 2(c)⁴³. The big trivial gap well separates the two spin sectors, enabling spin-polarized state, while the smaller non-trivial gap may give rise to topological insulating state like Chern insulator, when the Fermi level is placed there. The spin canting therefore induces what can be considered a non-relativistic spin splitting that does not distinguish between different d -orbitals, therefore preserving the orbital degeneracy and the simple profile of the band structure, at least in the isotropic limit. This renders canted spin order a very promising platform to realize fascinating topological phases of matter.

Real Space and Momentum Space Effective Magnetic Fluxes.— The non-collinear spin order gives rise to an effective magnetic flux felt by the electron⁴⁴, via gauge field defined along the nearest-neighbor link a_{ij}

$$\Phi_{\Delta,\nabla} = \sum_{ij \in \Delta,\nabla} a_{ij} \equiv \oint \mathbf{a} \cdot d\mathbf{r} = \int d\mathcal{S} \cdot (\nabla \times \mathbf{a}) \quad (2)$$

where the sum is over nearest neighbor links around an up or down triangle, \mathbf{a} is the continuous form of the gauge field vector, $d\mathbf{r}$ defines the path along the triangle, and \mathcal{S} is the surface normal vector. Representing the local spin \mathbf{S} corresponding to the magnetic moment vector \mathbf{M} in Eq.(1) by $\mathbf{S}(\mathbf{r}) = S(\sin \theta_{\mathbf{r}} \cos \phi_{\mathbf{r}}, \sin \theta_{\mathbf{r}} \sin \phi_{\mathbf{r}}, \cos \theta_{\mathbf{r}})$, computation based on spin coherent states⁴⁵ gives the gauge field for $s = 1/2$ (electron)¹⁹

$$a_{\mathbf{r}\mathbf{r}'} = -\tan^{-1} \left[\frac{\sin(\phi_{\mathbf{r}'} - \phi_{\mathbf{r}}) \sin \frac{\theta_{\mathbf{r}}}{2} \sin \frac{\theta_{\mathbf{r}'}}{2}}{\cos \frac{\theta_{\mathbf{r}}}{2} \cos \frac{\theta_{\mathbf{r}'}}{2} + \cos(\phi_{\mathbf{r}'} - \phi_{\mathbf{r}}) \sin \frac{\theta_{\mathbf{r}}}{2} \sin \frac{\theta_{\mathbf{r}'}}{2}} \right] \quad (3)$$

where $\mathbf{r} = (x_i, y_i)$, $\mathbf{r}' = (x_j, y_j)$, denotes the position vector of a lattice site and $a_{ij} \equiv a_{\mathbf{r}\mathbf{r}'}$. For coplanar 120° non-collinear spin order, $\theta_{\mathbf{r}} = \theta_{\mathbf{r}'} = \pi, \phi_{\mathbf{r}'} - \phi_{\mathbf{r}} = 2\pi/3$, the gauge field simplifies to $a_{\mathbf{r}\mathbf{r}'} = -\pi/3$, which gives $\Phi_{\Delta,\nabla} = -\pi$, which is a trivial, time-reversal symmetry-invariant phase angle because $\exp(i\pi) = \exp(-i\pi)$ ¹². This result suggests that coplanar non-collinear spin order alone does not give any nontrivial flux that breaks time-reversal symmetry. On the other hand, non-coplanar spin order easily gives nontrivial flux ($\Phi_{\Delta,\nabla} \neq 0, \pm\pi$). Taking $\phi_{\mathbf{r}'} - \phi_{\mathbf{r}} = 2\pi/3$ as before while taking $\theta_{\mathbf{r}} = \theta_0$ for all sites, we obtain $a_{\mathbf{r}\mathbf{r}'} = -\tan^{-1} \left(\sqrt{3} \tan^2 \frac{\theta_0}{2} / \left(2 - \tan^2 \frac{\theta_0}{2} \right) \right)$. This gauge field gives a nontrivial effective flux that can be associated with (scalar) spin chirality, defined as⁴⁶⁴⁷

$$\chi = \mathbf{S}_i \cdot (\mathbf{S}_j \times \mathbf{S}_k) = -\frac{\sqrt{3}}{2} S^3 \cos \theta_0 \quad (4)$$

where i, j, k label three spins on a triangle and $\theta_i = \theta_0$ for the three sublattices. Noting the vectorial expression of the scalar spin chirality, it is clear that this quantity vanishes for coplanar non-collinear spin order as well as ferromagnetic

order. Interestingly, the scalar spin chirality χ changes sign when one flips the canting from above to below the plane or vice versa; i.e. $\theta_0 \rightarrow \pi - \theta_0$. One can thus expect two degenerate states corresponding to opposite chiralities, which may have related topological character, to be found later.

QAHE is characterized by nonzero Chern number, a topological invariant of the band structure. To compute the Chern number, one first calculates the Berry curvature $\Omega(\mathbf{k})$ defined in momentum space²²²⁴ which for arbitrary temperature T is given by¹

$$\Omega(\mathbf{k}) = \hbar^2 \sum_{n \neq n'} G_{nn'}(\mathbf{k}) \text{Im} \left[\frac{\langle \psi_{n\mathbf{k}} | v_x(\mathbf{k}) | \psi_{n'\mathbf{k}} \rangle \langle \psi_{n'\mathbf{k}} | v_y(\mathbf{k}) | \psi_{n\mathbf{k}} \rangle}{(\epsilon_{n'\mathbf{k}} - \epsilon_{n\mathbf{k}})^2} \right] \quad (5)$$

with

$$G_{nn'}(\mathbf{k}) = f(\epsilon_n(\mathbf{k})) - f(\epsilon_{n'}(\mathbf{k})) \quad (6)$$

where $f(\epsilon_n(\mathbf{k})) = (\exp(\beta(\epsilon_n(\mathbf{k}) - E_F)) + 1)^{-1}$ with $\beta = 1/(k_B T)$ involving the Boltzmann constant k_B and reduced Planck constant \hbar . The Im implies the imaginary part, while $\psi_{n\mathbf{k}}, \epsilon_{n\mathbf{k}}$ respectively represent the eigenfunction and eigenvalue of the n^{th} -eigenstate of the Hamiltonian $H_{\mathbf{k}}$. The velocity operator is given by $v_{x(y)}(\mathbf{k}) = (1/\hbar) \partial H_{\mathbf{k}} / \partial k_{x(y)}$.

The Chern number is then simply given by the integral of Berry curvature over the Brillouin zone

$$C = \frac{1}{2\pi} \int_{\text{BZ}} d^2\mathbf{k} \Omega(\mathbf{k}) = \frac{\Phi_B}{2\pi} \quad (7)$$

associated to the reciprocal-space Berry phase Φ_B ²², which is the intrinsic origin of Hall conductivity $\sigma_{xy} = (e^2/h)C$ involving elementary charge e of the electron and Planck constant h .

QAHE from Canted Antiferromagnetic Order.—We first look at the Berry curvature, from a representative set of parameters that gives the most remarkable quantum anomalous Hall effect detailed later, as that used in Fig.2(c). As shown in Fig. 3, the Berry curvature can have different profiles, with different regions in the Brillouin zone with the peak magnitude of $\Omega(\mathbf{k})$. It can be checked by direct comparison with Fig.2(c) that such dominant region corresponds to the spot where the nontrivial gap is tightest, because that is where the curvature of the band is largest.

Next, the Chern number computed numerically exactly from the full 30×30 Hamiltonian matrix using Eq.(5). The resulting profile of the Chern number is shown in Fig. 4 as function of the Fermi energy. The value of the computed invariant is not quantized within the band, representing classical anomalous Hall conductivity from intrinsic Berry curvature mechanism. For the topological invariant to be integer (Chern number), the Fermi energy has to be within the gap, giving quantized Hall conductivity $\sigma_{xy} = Ce^2/h$ where C is the Chern number, e electron charge, and h is the Planck constant. For non-collinear coplanar spin order with isotropic Slater-Koster integrals, $C = 0$ everywhere, and remains to be so even with anisotropic Slater-Koster integrals, because the net magnetization is zero. Within our minimal model Eq.(1), nonzero C requires non-coplanar non-collinear spin order.

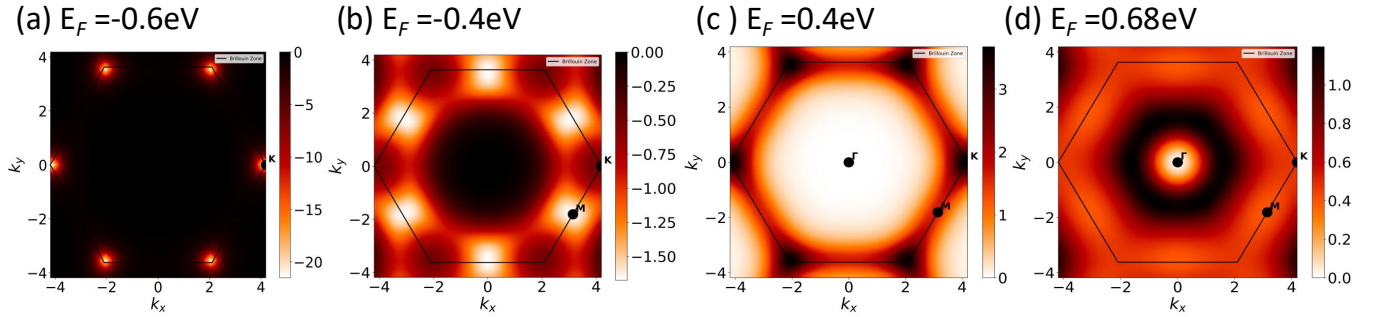


FIG. 3. Heat maps of the Berry curvature field $\Omega(k_x, k_y)$ in dimensionless form, with the same parameters as those for Fig. 2c) evaluated at a) $E_F = -0.60\text{eV}$ b) $E_F = -0.4\text{eV}$ in the spin up sector and c) $E_F = 0.4\text{eV}$ d) $E_F = 0.68\text{eV}$ for the spin down sector, within the gaps of the band structure in Fig. 2(c).

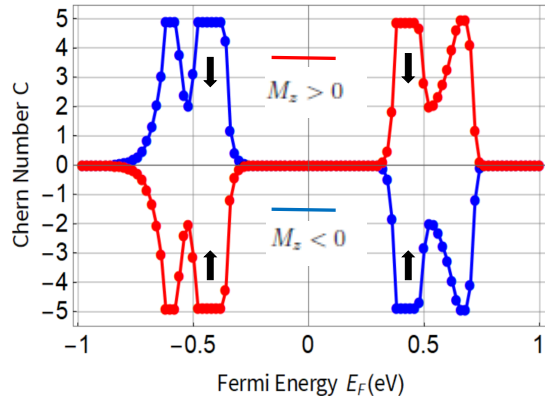


FIG. 4. The dependence of the Chern number C on the Fermi energy E_F (eV) at $T = 0.0001\text{eV} (= 1.1\text{Kelvin})$ for kagome d -electron system with 120° canted (non-coplanar) antiferromagnetic order, with parameters of Fig. 2(c), with $M_z = 0.6\text{eV}$ (red) and $M_z = -0.6\text{eV}$ (blue), giving a record value of large Chern number $C = \pm 5$ which simply flips sign when the sign of M_z is flipped. The dots are numerical data while the solid lines are guides to the eyes. The arrows mark the spin sectors (up or down).

Indeed, for non-coplanar (canted) non-collinear spin order, even with isotropic Slater-Koster integrals gives nonzero Chern number. As noted earlier, canted spin order possesses nonzero scalar spin chirality. When the onsite energy is equal for all the five d -orbitals, one obtains the relatively large $C = \pm 5$. This is five times larger than the Chern number found in ferromagnetic kagome system⁴⁹⁵⁰. The factor of 5 simply comes from the fact that all the five d orbitals contribute equally to the total Chern number. As far as we are aware of, this is the largest value of Chern number known so far in kagome electron system, which can occur naturally without requiring relativistic interaction⁵³ or heterostructure engineering⁵⁴. In addition, Fig. 4 shows that the two spin sectors carry Chern number of opposite signs. These opposite signs correspond to the opposite signs of scalar spin chiralities with polar angles θ_0 and $\pi - \theta_0$, as already hinted at early on by Eq.(4). Tuning the Fermi energy (filling factor), one can switch on or off one of the two counter propagating chiral edge states of a given spin state, realizing half of the edge

states of the quantum spin Hall effect⁵¹ in two dimensions.

Low-Energy Theory and Topological Transition.—To gain conceptual insight beyond numerical results, in particular on how such large Chern number $|C| = 5$ may arise in d -orbital system, we derive the low-energy effective theory of the d -electron around the Dirac point at K ⁴¹, which when expressed in terms of wave vector $\mathbf{q} = \mathbf{k} - \mathbf{K}$ gives

$$h_{\text{MassiveDirac}}(\mathbf{q}) = \sigma_0 \left[h(\mathbf{K}) + \frac{\sqrt{3}}{8} t \left(q_x J_x + \sqrt{3} q_y J_y \right) \right] - \frac{\hbar}{2} (\boldsymbol{\sigma} \cdot \mathbf{M}_J) \quad (8)$$

taking the form of a massive Dirac Hamiltonian with bare Fermi velocity $v_F^x = \sqrt{3}t/8$ along x and $v_F^y = 3t/8$ along y , where $h(\mathbf{K})$ is a constant 3×3 Hamiltonian matrix evaluated at \mathbf{K} where the Dirac point is located (in the absence of spin order)

$$h(\mathbf{K}) = \frac{t}{2} \begin{pmatrix} 0 & -1 & 1 \\ -1 & 0 & 1 \\ 1 & 1 & 0 \end{pmatrix} \quad (9)$$

and $t = V_{dd}\sigma = V_{dd}\delta = V_{dd}\pi$ in isotropic limit, J_x, J_y are 3×3 matrices defined in the sublattice A, B, C space,

$$J_x = \begin{pmatrix} 0 & -2 & -1 \\ -2 & 0 & -1 \\ -1 & -1 & 0 \end{pmatrix}, J_y = \begin{pmatrix} 0 & 0 & 1 \\ 0 & 0 & -1 \\ 1 & -1 & 0 \end{pmatrix}. \quad (10)$$

The $\boldsymbol{\sigma} = (\sigma_x, \sigma_y, \sigma_z)$ is the Pauli spin matrix vector, and \mathbf{M}_J is the magnetization vector matrix written in the sublattice space,

$$\mathbf{M}_J = (M_J^x, M_J^y, M_J^z)$$

$$= \left(\frac{\sqrt{3}}{2} M_{\perp} (J_A - J_B), M_{\perp} \left(J_C - \frac{J_A + J_B}{2} \right), J_0 M_z \right) \quad (11)$$

where $M_{\perp} = \sqrt{M_x^2 + M_y^2}$ and J_0, J_A, J_B, J_C are diagonal matrices defined in the sublattice space with matrix element $(J_0)_{ij} = \delta_{ij}$, $(J_A)_{ij} = \delta_{ij}\delta_{iA}$ and similarly for J_B, J_C .

To compute the Hall conductivity (or Chern number) from the low-energy Hamiltonian Eq.(8), we diagonalize the low-energy Hamiltonian in the sublattice space and then rewrite it in a generic form in the spin space⁵²

$$(h_{\text{Dirac}}(\mathbf{q}))_{\tilde{i}\tilde{j}} = \left(E_{\tilde{i}}(\mathbf{q})\sigma_0 + V_{\tilde{i}}\sigma_{\alpha}d_{\alpha}^{\tilde{i}}(\mathbf{q}) \right) \delta_{\tilde{i}\tilde{j}} \quad (12)$$

where the subscript indices $\tilde{i}, \tilde{j} = 1, 2, 3$ indicates matrix element in the diagonalized sublattice space, a directional vector $\mathbf{d}^{\tilde{i}}(\mathbf{k})$ with components $d_{\alpha}^{\tilde{i}}(\mathbf{q}), \alpha = x, y, z$ has been defined; a generic vector that depends on the wave vector $\mathbf{q} = \mathbf{k} - \mathbf{K}$. Our calculation gives $\mathbf{d}^{\tilde{i}}(\mathbf{q}) = (d_x^{\tilde{i}}(\mathbf{q}), d_y^{\tilde{i}}(\mathbf{q}), -\hbar M_z/2)$, where $d_x^{\tilde{i}}(\mathbf{q}), d_y^{\tilde{i}}(\mathbf{q})$ are even in M_z with rather complicated analytical expressions⁴¹.

Topological consideration shows that the Chern number can be expressed as $C = -(1/(4\pi)) \int_{\text{FBZ}} d^2\mathbf{q} \hat{\mathbf{d}}^{\tilde{i}}(\mathbf{q}) \cdot (\partial_{q_x} \hat{\mathbf{d}}^{\tilde{i}}(\mathbf{q}) \times \partial_{q_y} \hat{\mathbf{d}}^{\tilde{i}}(\mathbf{q}))$ where FBZ refers to the first Brillouin zone, $\hat{\mathbf{d}}^{\tilde{i}}(\mathbf{q}) = \mathbf{d}^{\tilde{i}}(\mathbf{q})/|\mathbf{d}^{\tilde{i}}(\mathbf{q})|$, and $\partial_{q_x(q_y)} = \partial/\partial q_{x(y)}$ ⁵². Noting that $d_z^{\tilde{i}}(\mathbf{q}) = -\hbar M_z/2$ independent of \mathbf{q} , this gives $C = -(4\pi)^{-1} \int_{\text{FBZ}} d^2\mathbf{q} \hat{d}_z^{\tilde{i}}(\mathbf{q}) \left(\partial_{q_x} d_x^{\tilde{i}}(\mathbf{q}) \partial_{q_y} d_y^{\tilde{i}}(\mathbf{q}) - \partial_{q_x} d_y^{\tilde{i}}(\mathbf{q}) \partial_{q_y} d_x^{\tilde{i}}(\mathbf{q}) \right)$. This suggests that the Chern number C should change sign when the sign of M_z changes⁴¹. This analytical finding perfectly agrees with the numerical result presented in Fig. 4, indicating a topological transition (a sign change of the Chern number) with the flipping of the M_z .

To find an explicit dependence of the Chern number on an appropriately defined effective gap of the system, we adopt the result of semiclassical Boltzmann equation and Kubo formalism⁵⁵, giving (from each d orbital)

$$C = \frac{\Delta}{\sqrt{\Delta^2 + 4\hbar^2 \left((\tilde{v}_F^x q_x^F)^2 + (\tilde{v}_F^y q_y^F)^2 \right)}} \Big|_{q_{x(y)}^F=0} = \text{sign}(\Delta) \quad (13)$$

where $\text{sign}(\Delta)$ means the sign of the gap Δ and we have put the Fermi energy to zero (the energy of massless of Dirac point) to get the last equality. The computed gap Δ turns out to have a given sign in each hemisphere of Bloch sphere while changing its sign as one cross the equator $\theta = \pi/2$, confirming the conclusion from topological consideration⁴¹. For θ close to equator, one obtains a simple expression for real space spin Berry phase from continuum formula⁴⁵ $\Phi = s \oint d\tau \phi(1 - \cos \theta) = \pi(1 - \cos \theta)$ for $s = 1/2$, which asymptotically reproduces the $\Phi_{\Delta, \nabla}$ from Eqs.(2-3) in the limit of $|\tan \theta| \rightarrow \infty$. Using the result from the flux model in kagome¹², the Chern number in the case with five-fold degeneracy (equal onsite energy for all the five d -orbitals) is given by

$$C = \pm 5 \text{sign}[\sin \pi(1 - \cos \theta)] \quad (14)$$

for Fermi energies within the nontrivial gap, where \pm is for the upper (lower) band sector.

To complete the analysis, the onsite energy simply shifts around the ± 1 Chern contribution of each d -orbital. In real materials, the onsite energies may differ for different orbitals,

allowing diverse possibilities $C = \pm 1, \pm 2, \pm 3, \pm 4, \pm 5$, but the Chern numbers must always sum up to $C = \pm 5$. The predicted largest Chern number $|C| = 5$ persists even at as large as 80% anisotropy in the Slater-Koster integrals⁴¹.

Discussion and Conclusions.—Our article reports the theoretical demonstration of quantum anomalous Hall effect from canted antiferromagnet from d -orbital electrons in kagome lattice. The necessary spin splitting in electronic band structure comes from the real space effective field induced by the spin texture with nonzero (scalar) spin chirality. In a sense, the predicted phenomenon is a quantum and antiferromagnetic version of topological Hall effect, originally proposed in classical system from magnetization texture in ferromagnet¹⁸. Equally importantly, our calculations suggest that the predicted large Chern number from canted spin configuration is robust even for relatively strong anisotropy in the Slater-Koster integrals, thus potentially describing real materials. Pairs of plateaus of Chern numbers with opposite signs emerge with spin-momentum locking, which flip sign when M_z is flipped, corresponding to opposite scalar spin chiralities. The canted spin order induces topological gap that does not discriminate different d -orbitals, resulting in quantum anomalous Hall effect with large Chern numbers that can be tuned by varying the onsite energies.

Acknowledgements.—I.M. thanks M. Diouf, N. and R. Saidi, M. Ngom, C. Ngbo-Tiba Guiguisia, and M. Beye for the numerous discussions during their internship with the author which inspired the latter to pursue and complete this work. W. A. acknowledges the doctoral funding from Aix-Marseille Université that financially supports the author in this research. I. M. conceived the idea and the plan for the project. W. A., I. M., S.S., and R.H. performed the numerical calculations, while I.M. and P. L. derived the analytical results. All of the authors were involved in the analysis of the results and writing of the manuscript.

- ¹N. Nagaosa, J. Sinova, S. Onoda, A. H. MacDonald, and N. P. Ong, Anomalous Hall effect, Rev. Mod. Phys. 82, 1539 (2010).
- ²T. Neupert, L. Santos, C. Chamon, and C. Mudry, Fractional Quantum Hall States at Zero Magnetic Field, Phys. Rev. Lett. 106, 236804 (2011).
- ³K. Sun, Z. Gu, H. Katsura, and S. Das Sarma, Nearly-flat bands with nontrivial topology, Phys. Rev. Lett. 106, 236803 (2011).
- ⁴E. Tang, J.-W. Mei, and X.-G. Wen, High temperature fractional quantum Hall states, Phys. Rev. Lett. 106, 236802 (2011).
- ⁵M. Kang, L. Ye, S. Fang, J.-S. You, A. Levitan, M. Han, J. I. Facio, C. Jozwiak, A. Bostwick, E. Rotenberg, M. K. Chan, R. D. McDonald, D. Graf, K. Kaznatcheev, E. Vescovo, D. C. Bell, E. Kaxiras, J. van den Brink, M. Richter, M. P. Ghimire, J. G. Checkelsky, and R. Comin, Dirac fermions and flat bands in the ideal kagome metal FeSn, Nat. Mater. 19, 163 (2020).
- ⁶I. Makhfudz, Fluctuation-induced First Order Quantum Phase Transition of U(1) Quantum Spin Liquid in Pyrochlore Quantum Antiferromagnet, Phys. Rev. B 89, 024401 (2014).
- ⁷L. Savary and L. Balents, Quantum Spin Liquids, Rep. Prog. Phys. 80, 016502 (2017).
- ⁸Taguchi Y, Oohara Y, Yoshizawa H, Nagaosa N, and Tokura Y., Spin Chirality, Berry Phase, and Anomalous Hall Effect in a Frustrated Ferromagnet, Science 291(5513), 2573 (2001).
- ⁹J. Ye, Y. B. Kim, A. J. Millis, B. I. Shraiman, P. Majumdar, and Z. Tešanović, Berry phase theory of the Anomalous Hall Effect: Application to Colossal Magnetoresistance Manganites, Phys. Rev. Lett. 83, 3737 (1999).
- ¹⁰S. Onoda and N. Nagaosa, Spin Chirality Fluctuation and Anomalous Hall Effect in Itinerant Ferromagnets, Phys. Rev. Lett. 90, 196602 (2003).

¹¹I. Martin and C. D. Batista, Scalar spin chirality and quantum Hall effect on triangular lattice, *Phys. Rev. Lett.* 101, 156402 (2008).

¹²Ohgushi K., Murakami S., Nagaosa N., Spin Anisotropy and Quantum Hall Effect in the Kagome Lattice - Chiral Spin State based on a Ferromagnet, *Phys. Rev. B* 62, R6065 (2000).

¹³Z. Fang, N. Nagaosa, K. S. Takahashi, A. Asamitsu, R. Mathieu, T. Ogasawara, H. Yamada, M. Kawasaki, Y. Tokura, and K. Terakura, The Anomalous Hall Effect and Magnetic Monopoles in Momentum Space, *Science* 302, 92 (2003).

¹⁴M. Taillefumier, B. Canals, C. Lacroix, V. K. Dugaev, and P. Bruno, Anomalous Hall effect due to spin chirality in the Kagomé lattice, *Phys. Rev. B* 74, 085105 (2006).

¹⁵H. Chen, Q. Niu, and A. H. MacDonald, Anomalous Hall Effect Arising from Noncollinear Antiferromagnetism, *Phys. Rev. Lett.* 112, 017205 (2014).

¹⁶A. K. Nayak, J. E. Fischer, Y. Sun, B. Yan, J. Karel, A. C. Komarek, C. Shekhar, N. Kumar, W. Schnelle, J. Kubler, C. Felser, and S. S. P. Parkin, Large anomalous Hall effect driven by a nonvanishing Berry curvature in the noncollinear antiferromagnet Mn₃Ge, *Sci. Adv.* 2, e1501870 (2016).

¹⁷S. Nakatsuji, N. Kiyohara, and T. Higo, Large anomalous Hall effect in a non-collinear antiferromagnet at room temperature, *Nature (London)* 527, 212 (2015).

¹⁸P. Bruno, V. K. Dugaev, and M. Taillefumier, Topological Hall Effect and Berry Phase in Magnetic Nanostructures, *Phys. Rev. Lett.* 93, 096806 (2004).

¹⁹I. Makhfudz and P. Pujol, Protection against Spin Gap in 2-d Insulating Antiferromagnets with a Chern-Simons Term, *Phys. Rev. B* 92, 144507 (2015).

²⁰G. Sundaram and Q. Niu, Wave-packet dynamics in slowly perturbed crystals: Gradient corrections and Berry-phase effects, *Phys. Rev. B* 59, 14 915 (1999).

²¹N. A. Sinitsyn, Semiclassical theories of the anomalous Hall effect, *J. Phys.: Cond. Matt.* 20 (2008) 023201.

²²F. D. M. Haldane, Berry Curvature on the Fermi Surface: Anomalous Hall Effect as a Topological Fermi-Liquid Property, *Phys. Rev. Lett.* 93, 206602 (2004).

²³C-Z. Chang, C-X. Liu, and A. H. MacDonald, Colloquium: Quantum anomalous Hall effect, *Rev. Mod. Phys.* 95, 011002 (2023).

²⁴D. J. Thouless, M. Kohmoto, M. P. Nightingale, and M. den Nijs, Quantized Hall Conductance in a Two-Dimensional Periodic Potential, *Phys. Rev. Lett.* 49, 405 (1982).

²⁵F. D. M. Haldane, Model for a Quantum Hall Effect without Landau Levels: Condensed-Matter Realization of the "Parity Anomaly", *Phys. Rev. Lett.* 61, 2015 (1988).

²⁶M. Onoda and N. Nagaosa, Quantized Anomalous Hall Effect in Two-Dimensional Ferromagnets: Quantum Hall Effect in Metals, *Phys. Rev. Lett.* 90, 206601 (2003).

²⁷K. Sun, H. Yao, E. Fradkin, and S. A. Kivelson, Topological Insulators and Nematic Phases from Spontaneous Symmetry Breaking in 2D Fermi Systems with a Quadratic Band Crossing, *Phys. Rev. Lett.* 103, 046811 (2009).

²⁸Z. Qiao, W. Ren, H. Chen, L. Bellaiche, Z. Zhang, A. H. MacDonald, and Q. Niu, Quantum Anomalous Hall Effect in Graphene Proximity Coupled to an Antiferromagnetic Insulator, *Phys. Rev. Lett.* 112, 116404 (2014).

²⁹P. Högl, T. Frank, K. Zollner, D. Kochan, M. Gmitra, and J. Fabian, Quantum Anomalous Hall Effects in Graphene from Proximity-Induced Uniform and Staggered Spin-Orbit and Exchange Coupling, *Phys. Rev. Lett.* 124, 136403 (2020).

³⁰C-X. Liu, X-L. Qi, X. Dai, Z. Fang, and S-C. Zhang, Quantum Anomalous Hall Effect in Hg(1-y)Mn(y)Te Quantum Wells, *Phys. Rev. Lett.* 101, 146802 (2008).

³¹C-X. Liu, S-C. Zhang, and X-L. Qi, The Quantum Anomalous Hall Effect: Theory and Experiment, *Annu. Rev. Condens. Matter Phys.* 7, 301 (2016).

³²C-Z. Chang, J. Zhang, X. Feng, J. Shen, Z. Zhang, M. Guo, K. Li, Y. Ou, P. Wei, L-L. Wang, Z-Q. Ji, Y. Feng, S. Ji, X. Chen, J. Jia, X. Dai, Z. Fang, S-C. Zhang, K. He, Y. Wang, L. Lu, X-C. Ma, and Q-K. Xue, Experimental Observation of the Quantum Anomalous Hall Effect in a Magnetic Topological Insulator, *Science* 340, 167 (2013).

³³Deng, Y., Yu, Y., Shi, M. Z., Guo, Z., Xu, Z., Wang, J., Chen, X.H., and Zhang, Y., Quantum anomalous Hall effect in intrinsic magnetic topological insulator MnBi₂Te₄, *Science* 367, 895 (2020).

³⁴I. Makhfudz, M. Cherkasskii, M. Alipourzadeh, Y. Hajati, P. Lombardo, S. Schäfer, S. V. Kusminskiy, and R. Hayn, Quantum anomalous Hall effect in *d*-electron kagome systems: Chern insulating states from transverse spin-orbit coupling, *Phys. Rev. B* 110, 235130 (2024).

³⁵V. Baltz, A. Manchon, M. Tsai, T. Moriyama, T. Ono, and Y. Tserkovnyak, Antiferromagnetic spintronics, *Rev. Mod. Phys.* 90, 015005 (2018).

³⁶S. Sachdev, Kagome' and triangular-lattice Heisenberg antiferromagnets: Ordering from quantum fluctuations and quantum-disordered ground states with unconfined bosonic spinons, *Phys. Rev. B* 45, 12377 (1992).

³⁷J. Kipp, K. Samanta, F. R. Lux, M. Merte, J.-P. Hanke, M. Redies, F. Freimuth, S. Blügel, M. Ležaić, Y. Mokrousov, The chiral Hall effect in canted ferromagnets and antiferromagnets, *Communications Physics* 4, 99 (2021).

³⁸H. Takagi, R. Takagi, S. Minami, T. Nomoto, K. Ohishi, M.-T. Suzuki, Y. Yanagi, M. Hirayama, N. D. Khanh, K. Karube, H. Saito, D. Hashizume, R. Kyanagi, Y. Tokura, R. Arita, T. Nakajima, and S. Seki, Spontaneous topological Hall effect induced by non-coplanar antiferromagnetic order in intercalated van der Waals materials, *Nature Physics* 19, 961 (2023).

³⁹X. Zhou, W. Feng, Y. Li, Y. Yao, Spin-Chirality-Driven Quantum Anomalous and Quantum Topological Hall Effects in Chiral Magnets, *Nano Lett.* 23, 5680 (2023).

⁴⁰W. A. Harrison, *Electronic Structure and the Properties of Solids: The Physics of the Chemical Bond* (Dover Publications, Inc., New York, United States (1980)).

⁴¹Please see the supplementary materials containing the derivation of low-energy Dirac Hamiltonian, the role of anisotropy in Slater-Koster integrals, canting angle, and onsite energy. These materials also make reference to ⁵².

⁴²M. Kang, L. Ye, S. Fang, J.-S. You, A. Levitan, M. Han, J. I. Facio, C. Jozwiak, A. Bostwick, E. Rotenberg, M. K. Chan, R. D. McDonald, D. Graf, K. Kaznatcheev, E. Vescovo, D. C. Bell, E. Kaxiras, J. van den Brink, M. Richter, M. P. Ghimire, J. G. Checkelsky, and R. Comin, Dirac fermions and flat bands in the ideal kagome metal FeSn, *Nat. Mater.* 19, 163 (2020).

⁴³Even though the non-collinear spin order mixes up spin up and spin down sectors, we will continue to use this phrase, implying in Fig.2(b-c) the upper group of bands as spin down (up) sector and lower group of bands as spin up (down) sector for $M_z > 0 (< 0)$, just like in ferromagnetic case³⁴.

⁴⁴I. Makhfudz and P. Pujol, Hole properties on and off magnetization plateaus in 2D antiferromagnets, *Phys. Rev. Lett.* 114, 087204 (2015).

⁴⁵A. Auerbach, *Interacting Electrons and Quantum Magnetism* (Springer, New York, United States (1994)).

⁴⁶X. G. Wen, Frank Wilczek, and A. Zee, Chiral spin states and superconductivity, *Phys. Rev. B* 39, 11413 (1989).

⁴⁷I. Makhfudz, Effective field theory of chiral spin liquid between ordered phases in a kagome antiferromagnet, *J. Phys.: Condens. Matter* 30, 225801 (2018).

⁴⁸S. Okamoto, N. Mohanta, E. Dagotto, and D. N. Sheng, Topological flat bands in a kagome lattice multiorbital system, *Communications Physics* 5, 198 (2022).

⁴⁹G. Xu, B. Lian, and S-C. Zhang, Intrinsic Quantum Anomalous Hall effect in Kagome lattice Cs₂LiMn₃F₁₂, *Phys. Rev. Lett.* 115, 186802 (2015).

⁵⁰L. Ye, M. Kang, J. Liu, F. von Cube, C. R. Wicker, T. Suzuki, C. Jozwiak, A. Bostwick, E. Rotenberg, D. C. Bell, L. Fu, R. Comin, and J. G. Checkelsky, Massive Dirac fermions in a ferromagnetic kagome metal, *Nature* 555, 638 (2018).

⁵¹C. L. Kane and E. J. Mele, Quantum Spin Hall Effect in Graphene, *Phys. Rev. Lett.* 95, 226801 (2005).

⁵²Qi, X. L., Wu, Y.-S., and Zhang, S.-C., Topological quantization of the spin Hall effect in two-dimensional paramagnetic semiconductors, *Phys. Rev. B* 74, 085308 (2006).

⁵³J. Wang, B. Lian, H. Zhang, Y. Xu, and S-C. Zhang, Quantum Anomalous Hall Effect with Higher Plateaus, *Phys. Rev. Lett.* 111, 136801 (2013).

⁵⁴C. Fang, M. J. Gilbert, and B. A. Bernevig, Large-Chern-Number Quantum Anomalous Hall Effect in Thin-Film Topological Crystalline Insulators, *Phys. Rev. Lett.* 112, 046801 (2014).

⁵⁵N. A. Sinitsyn, A. H. MacDonald, T. Jungwirth, V. K. Dugaev, and J. Sinova, Anomalous Hall effect in a two-dimensional Dirac band: The link between the Kubo-Streda formula and the semiclassical Boltzmann equation approach, *Phys. Rev. B* 75, 045315 (2007).

Supplementary Materials: Large Chern-Number Quantum Anomalous Hall Effect from Canted Antiferromagnetic Order in d -Electron System on Kagome Lattice

W. Ahmed¹, S. Schaeffer¹, P. Lombardo¹, R. Hayn¹, and I. Makhfudz¹

¹IM2NP, UMR CNRS 7334, Aix-Marseille Université, 13013 Marseille, France

In these Supplementary Materials, we provide additional details supplementing the main text. First, the derivation of low-energy theory reported in the main text to discuss the topological phase transition is provided. Then, supplemental results on the roles of onsite energy, robustness of the predicted large-Chern number QAHE on the anisotropy in the Slater-Koster integrals, and the dependence of QAHE on the canting angle are presented.

I. DERIVATION OF EFFECTIVE LOW-ENERGY HAMILTONIAN

We start from the kinetic part of the Hamiltonian in Fourier space, which takes the form of a 3×3 matrix defined in the sublattice space;

$$h(\mathbf{k}) = t \begin{pmatrix} 0 & \cos \mathbf{k} \cdot \mathbf{d}_{AB} & \cos \mathbf{k} \cdot \mathbf{d}_{CA} \\ \cos \mathbf{k} \cdot \mathbf{d}_{AB} & 0 & \cos \mathbf{k} \cdot \mathbf{d}_{BC} \\ \cos \mathbf{k} \cdot \mathbf{d}_{CA} & \cos \mathbf{k} \cdot \mathbf{d}_{BC} & 0 \end{pmatrix} \quad (15)$$

where $t = V_{dd\sigma} = V_{dd\delta} = V_{dd\pi}$ in isotropic limit and $\mathbf{d}_{AB}, \mathbf{d}_{AB}, \mathbf{d}_{AB}$ are nearest-neighbor unit vectors between two adjacent sites (or sublattices). Expanding the Hamiltonian around Dirac point, $\mathbf{k} = \mathbf{K} + \mathbf{q}$, we obtain

$$h(\mathbf{k}) = h(\mathbf{K}) + h(\mathbf{q}) \quad (16)$$

where $h(\mathbf{K})$ is a constant Hamiltonian once \mathbf{K} , where the Dirac point is located, is fixed as a reference. The unit cell triangle and the three sublattices (and the spin vector orientation for the co-planar collinear spin order assumed) are illustrated in Fig. 5. Expanding the cosine term to linear order in \mathbf{q} , e.g. $\cos(\mathbf{K} + \mathbf{q}) \cdot \mathbf{d}_{AB} = \cos \mathbf{K} \cdot \mathbf{d}_{AB} \cos \mathbf{q} \cdot \mathbf{d}_{AB} - \sin \mathbf{K} \cdot \mathbf{d}_{AB} \sin \mathbf{q} \cdot \mathbf{d}_{AB} \approx \cos \mathbf{K} \cdot \mathbf{d}_{AB} - \mathbf{q} \cdot \mathbf{d}_{AB} \sin \mathbf{K} \cdot \mathbf{d}_{AB}$, we obtain

$$h(\mathbf{K}) = \frac{t}{2} \begin{pmatrix} 0 & -1 & 1 \\ -1 & 0 & 1 \\ 1 & 1 & 0 \end{pmatrix} \quad (17)$$

for the constant Hamiltonian part and

$$h(\mathbf{q}) = t \begin{pmatrix} 0 & -\mathbf{q} \cdot \mathbf{d}_{AB} s_{AB} & -\mathbf{q} \cdot \mathbf{d}_{CA} s_{CA} \\ -\mathbf{q} \cdot \mathbf{d}_{AB} s_{AB} & 0 & -\mathbf{q} \cdot \mathbf{d}_{BC} s_{BC} \\ -\mathbf{q} \cdot \mathbf{d}_{CA} s_{CA} & -\mathbf{q} \cdot \mathbf{d}_{BC} s_{BC} & 0 \end{pmatrix} \quad (18)$$

where we have introduced a shorthand notation $s_{AB} = \sin \mathbf{K} \cdot \mathbf{d}_{AB}$ and similarly for the other two pairs of sublattices. The vectors $\mathbf{d}_{AB}, \mathbf{d}_{BC}, \mathbf{d}_{CA}$ can be deduced from Fig. 5. We will use a convention where the length of the nearest-neighbor vector is $1/2$ instead of 1 as used in³⁴. As such, the Dirac point is located at $\mathbf{K} = 4\pi/3$. The resulting linear in- \mathbf{q} part of the Hamiltonian becomes

$$h_{\text{Dirac}}(\mathbf{q}) = \frac{t}{2} \begin{pmatrix} 0 & -\frac{\sqrt{3}}{2} q_x & \frac{\sqrt{3}}{2} \left(-\frac{q_x}{2} + \frac{\sqrt{3}}{2} q_y \right) \\ -\frac{\sqrt{3}}{2} q_x & 0 & -\frac{\sqrt{3}}{2} \left(\frac{q_x}{2} + \frac{\sqrt{3}}{2} q_y \right) \\ \frac{\sqrt{3}}{2} \left(-\frac{q_x}{2} + \frac{\sqrt{3}}{2} q_y \right) & -\frac{\sqrt{3}}{2} \left(\frac{q_x}{2} + \frac{\sqrt{3}}{2} q_y \right) & 0 \end{pmatrix} \quad (19)$$

which can be simply written as

$$h_{\text{Dirac}}(\mathbf{q}) = \frac{\sqrt{3}}{8} t \left(q_x J_x + \sqrt{3} q_y J_y \right) \quad (20)$$

where the J matrices are given by

$$J_x = \begin{pmatrix} 0 & -2 & -1 \\ -2 & 0 & -1 \\ -1 & -1 & 0 \end{pmatrix}, J_y = \begin{pmatrix} 0 & 0 & 1 \\ 0 & 0 & -1 \\ 1 & -1 & 0 \end{pmatrix}. \quad (21)$$

The corresponding band structure of $h_{\text{Dirac}}(\mathbf{k}) = h(\mathbf{K}) + h_{\text{Dirac}}(\mathbf{q})$ is shown in Fig 6, displaying three bands; one of them is a flat band while the other two are dispersive bands with linear spectrum touching at a Dirac point.

Next, we consider the Zeeman term, which is off diagonal both in the spin and sublattice spaces

$$h_{\text{Zeeman}} = - \sum_{i \in A, B, C} \mathbf{M}_i \cdot \mathbf{s} \quad (22)$$

where $\mathbf{s} = (\hbar/2)\boldsymbol{\sigma}$, with $\boldsymbol{\sigma} = (\sigma_x, \sigma_y, \sigma_z)$ the Pauli spin matrices vector. Referring to the spin vectors represented by the arrows in Fig. 5, we have

$$h_{\text{Zeeman}} = -\frac{\hbar}{2} (J_0 \sigma_z M_z + \sigma_{\perp} \cdot (\mathbf{M}_{\perp}^A J_A + \mathbf{M}_{\perp}^B J_B + \mathbf{M}_{\perp}^C J_C)) \quad (23)$$

where we have added the uniform z part of magnetization; M_z to generalize the formulation to canted spin order (when $M_z = 0$ we recover the coplanar noncollinear spin order) while $\sigma_{\perp} = (\sigma_x, \sigma_y, 0)$ and $\mathbf{M}_{A\perp} = (M_x^A, M_y^A, 0) = M_{\perp}(\sqrt{3}/2, -1/2, 0)$ and similarly for the other two sublattices. The J matrices are given by

$$J_0 = \begin{pmatrix} 1 & 0 & 0 \\ 0 & 1 & 0 \\ 0 & 0 & 1 \end{pmatrix}, J_A = \begin{pmatrix} 1 & 0 & 0 \\ 0 & 0 & 0 \\ 0 & 0 & 0 \end{pmatrix}, J_B = \begin{pmatrix} 0 & 0 & 0 \\ 0 & 1 & 0 \\ 0 & 0 & 0 \end{pmatrix}, J_C = \begin{pmatrix} 0 & 0 & 0 \\ 0 & 0 & 0 \\ 0 & 0 & 1 \end{pmatrix}. \quad (24)$$

Defining massive Dirac Hamiltonian

$$h_{\text{MassiveDirac}}(\mathbf{q}) = h(\mathbf{K}) + h_{\text{Dirac}}(\mathbf{q}) + h_{\text{Zeeman}} = h_{\text{Dirac}}(\mathbf{k}) + h_{\text{Zeeman}} \quad (25)$$

which gives the following 6×6 Hamiltonian

$$h_{\text{MassiveDirac}}(\mathbf{q}) = \sigma_0 h(\mathbf{K}) + \frac{\sqrt{3}}{8} t (q_x J_x + \sqrt{3} q_y J_y) \sigma_0 - \frac{\hbar}{2} (\boldsymbol{\sigma} \cdot \mathbf{M}_J) \quad (26)$$

where σ_0 is 2×2 identity matrix defined in the spin space and the 3×3 matrix vector \mathbf{M}_J defined in the sublattice space has the following elements

$$\mathbf{M}_J = (M_J^x, M_J^y, M_J^z) = \left(\frac{\sqrt{3}}{2} M_{\perp} (J_A - J_B), M_{\perp} \left(J_C - \frac{J_A + J_B}{2} \right), J_0 M_z \right) \quad (27)$$

giving a massive Dirac fermion Hamiltonian, where the mass comes from the Zeeman (last) term in Eq.(26). Diagonalizing the Hamiltonian in the sublattice space, one obtains

$$h_{\text{MassiveDirac}}(\mathbf{q}) \rightarrow h_{\text{MassiveDirac}}^{\text{diag}}(\mathbf{q}) = U^{\dagger} h_{\text{Dirac}}(\mathbf{k}) U + U^{\dagger} h_{\text{Zeeman}} U \quad (28)$$

where U is a unitary orthogonal matrix $U^{\dagger} U = 1$. We choose U to diagonalize the $h(\mathbf{k})$ in the sublattice space, because h_{Zeeman} is already diagonal in this space. Therefore, it is guaranteed that $U^{\dagger} h_{\text{Zeeman}} U$ remains diagonal in the sublattice space. Doing so, one obtains

$$h_{\text{MassiveDirac}}^{\text{diag}}(\mathbf{q}) = \begin{pmatrix} E_{11}(\mathbf{q}) + V_1 \mathbf{d}^1(\mathbf{q}) \cdot \boldsymbol{\sigma} & 0 & 0 \\ 0 & E_{22}(\mathbf{q}) + V_2 \mathbf{d}^2(\mathbf{q}) \cdot \boldsymbol{\sigma} & 0 \\ 0 & 0 & E_{33}(\mathbf{q}) + V_3 \mathbf{d}^3(\mathbf{q}) \cdot \boldsymbol{\sigma} \end{pmatrix} \quad (29)$$

where $\boldsymbol{\sigma}$ is the Pauli spin matrix vector $\boldsymbol{\sigma} = (\sigma_x, \sigma_y, \sigma_z)$ and $\mathbf{d}^i(\mathbf{q}), i = 1, 2, 3$ is \mathbf{q} -dependent Bloch vector for each state.

The corresponding unit vector $\hat{\mathbf{d}}(\mathbf{q}) = \mathbf{d}(\mathbf{q})/|\mathbf{d}(\mathbf{q})|$ lives on Bloch sphere defined in \mathbf{k} space. The corresponding Hall conductivity can be computed from¹

$$\sigma_{xy} = -\frac{1}{8\pi^2} \int_{\text{FBZ}} d^2 \mathbf{q} \hat{\mathbf{d}}(\mathbf{q}) \cdot (\partial_{q_x} \hat{\mathbf{d}}(\mathbf{q}) \times \partial_{q_y} \hat{\mathbf{d}}(\mathbf{q})) \equiv \frac{e^2}{2\pi\hbar} C \quad (30)$$

where FBZ refers to the first Brillouin zone, the partial derivative is in \mathbf{q} space; $\partial_{q_x(q_y)} = \partial/\partial q_{x(y)}$ and we work with the units where $e = \hbar = 1$. The analytical expression for the vector $\mathbf{d}(\mathbf{q})$ is rather complicated as it involves the solution of a cubic polynomial equation, but can in principle be calculated from Eq.(26) with details given in the following paragraphs. It is to be noted that the integral in Eq.(30) resembles the Skyrmion number, which simply counts how many times the unit vector $\hat{\mathbf{d}}$ winds around the Bloch sphere in \mathbf{k} space as one sweeps the Brillouin zone. The Chern number can be determined by visualizing the

profile of $\hat{\mathbf{d}}$ vector and computing the solid angle it covers as one scans through the \mathbf{q} space. The corresponding Chern number is simply given by $C = S/(4\pi)$, where S is the area (solid angle) covered by the $\hat{\mathbf{d}}$ vector.

The constant prefactor V_i can always be absorbed into the vector $\mathbf{d}^i(\mathbf{q})$, thus giving us freedom to simply set the prefactor to unity. Doing so, the analytical expression for the components of $\mathbf{d}^i(\mathbf{q} = 0)$ vector is found to be, for $\tilde{i} = 1$

$$d_x^1(\mathbf{q} = 0) = \frac{2t^2 \operatorname{Re} \left(\frac{1}{(iM_p^3 - 2t^3 + \sqrt{-M_p^3(M_p^3 + 4it^3)})^{1/3}} \right)}{2 \times 2^{2/3}} + \frac{2 \operatorname{Re} \left(\left(iM_p^3 - 2t^3 + \sqrt{-M_p^3(M_p^3 + 4it^3)} \right)^{1/3} \right)}{4 \times 2^{1/3}}; \quad (31)$$

$$d_y^1(\mathbf{q} = 0) = \frac{-2 \operatorname{Im} \left[4t^2 \left(\frac{1}{(-iM_p^3 - 2t^3 + \sqrt{-M_p^6 + 4iM_p^3t^3})^{1/3}} \right) \right] - 4 \times 2^{1/3} \operatorname{Im} \left[\left(-iM_p^3 - 2t^3 + \sqrt{-M_p^6 + 4iM_p^3t^3} \right)^{1/3} \right]}{8 \times 2^{2/3}}; \quad (32)$$

$$d_z^1(\mathbf{q} = 0) = -\frac{\hbar M_z}{2} \quad (33)$$

where $\operatorname{Re}, \operatorname{Im}$ represent the real part and the imaginary part, respectively. Similar expression can be derived for $\tilde{i} = 2, 3$. We have denoted $M_p \equiv M_\perp = \sqrt{M_x^2 + M_y^2}$ which is subject to the constraint $M_z^2 + M_p^2 = M_s^2$ with fixed M_s . Eventually, $d_z^i(\mathbf{q}) = -\hbar M_z/2$ for all $\tilde{i} = 1, 2, 3$, independent of \mathbf{q} . As such, the integral in Eq.(30) can be written explicitly as

$$C = -\frac{1}{4\pi} \int_{\text{FBZ}} d^2\mathbf{q} d_z^i(\mathbf{q}) \left(\partial_{q_x} d_x^i(\mathbf{q}) \partial_{q_y} d_y^i(\mathbf{q}) - \partial_{q_x} d_y^i(\mathbf{q}) \partial_{q_y} d_x^i(\mathbf{q}) \right) \quad (34)$$

which clearly changes sign when we changes the sign of M_z , noting Eq.(33). In other words, in canted spin order, the Chern number must be an odd function of M_z .

When one tunes the direction of the magnetic moment \mathbf{M}_i from coplanar in the xy plane to collinear along z or vice versa, the band structure deforms dramatically. This is because such reorientation of the direction of the moment amounts to, rather than a small perturbation, a large deformation of the Hamiltonian. The bands are not simply gradually moved away or closer to each other, but rearranged completely. Therefore, it becomes more subtle how to define a gap, starting from the energy eigenvalues of the Hamiltonian. But as described in the main text and as deduced above, the topological properties actually do not depend on the actual size of the gap, but only on its “sign”, which reflects the relative positioning of the bands relative to each other. When the bands get inverted; i.e. when “band inversion” occurs, the topological properties may change. We therefore define the gap Δ by choosing the simplest possible convention; defined in terms of the intra-pair gap,

$$E_g^{\tilde{i}} = E_{\tilde{i}}^+ - E_{\tilde{i}}^- = 2|\mathbf{d}^{\tilde{i}}| \quad (35)$$

where $\tilde{i} = 1, 2, 3$. The gap however must be odd with the change of sign of M_z . So, we define the gap to be

$$\Delta = \operatorname{sign}(M_z) (E_g^{\tilde{i}} - |M_z|) \quad (36)$$

where $|M_z|$ indicates the absolute value of M_z . The profile of this gap is shown in Fig. 7. The main feature of this gap is that it does not change sign as one varies M_z in the northern hemisphere $M_z > 0$ and southern hemisphere $M_z < 0$ of the Bloch sphere; it only changes sign at the equator $M_z = 0$. Note that this gap does not represent the tiny nontrivial gap between nearly-touching bands at the initially Dirac point or quadratic band crossing point. Rather, it represents the gap between spin up and spin down sectors of a given sublattice state, normalized with respect to the z part of Zeeman field M_z . This result predicts that the Chern number remains robust, as long as the gap is non-zero and not overshadowed by any band, as one tune the angle of the canting, and the Chern number changes sign only when the canting passes the equator. This prediction is confirmed numerically in Section II of the Supplementary Materials.

II. ADDITIONAL RESULTS

A. The Role of Onsite Energies: Switch of Topological Phase Transition

Onsite energies can be used as a switch to split the $C = \pm 5$ Chern peaks into different series of lower Chern number peaks. This is illustrated in Fig. 9 where two different Chern series, the so-called 1-2-2 series and 3-2 series are obtained by judiciously

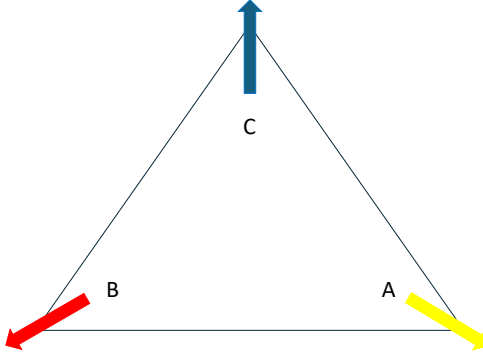


FIG. 5. The unit cell of a kagome lattice with its three sublattices and the corresponding spin vectors.

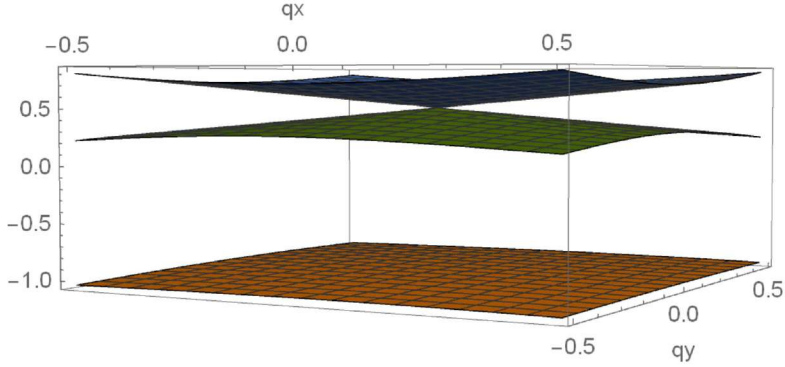


FIG. 6. Band structure of low-energy Hamiltonian $h(\mathbf{K}) + h_{\text{Dirac}}(\mathbf{q})$ with its Dirac point.

setting the onsite energies to have corresponding degeneracies. In a sense, the onsite energy can therefore be regarded as a switch of a topological phase transition that changes the Chern number of the quantum anomalous Hall state, corresponding to the number of chiral edge states present at a given Fermi energy. So far, we have assumed degeneracy in terms of onsite energy for d -orbitals of the same symmetry; between d_{xz} and d_{yz} orbitals, and also between d_{xy} and $d_{x^2-y^2}$ orbitals. In the most general case, these orbitals are not necessarily degenerate in onsite energy; their onsite energies are split, which can be caused by orbital rotation due to crystal field splitting for example. In this case, the splitting follows certain symmetry described in Section II of these supplementary materials. We reserve this more complicated case for future work.

B. Robustness of $|C = 5|$ QAHE with Anisotropy in Slater-Koster Integrals

In the main text, we have presented results mainly based on our model assuming isotropic Slater-Koster integrals. This is a very idealized situation; in real materials, Slater-Koster integrals that would fit first-principle band structure would in general be anisotropic. Question naturally arise whether the predicted results coming from isotropic limit would be applicable to any real materials.

To answer this question, we hereby present the result of test calculations with anisotropic Slater-Koster integrals. The band structures for different cases with canted spin order but with different amounts of anisotropy in the Slater-Koster integrals are presented in Fig. 12. Starting from $V_{dd\pi} = V_{dd\delta} = V_{dd\sigma} = -0.25\text{eV}$ in the isotropic limit, with clear $C = \pm 5$ Chern peaks, we make the V_{dd} 's anisotropic by (a) 20%; $V_{dd\pi} = -0.25\text{eV}$, $V_{dd\delta} = -0.30\text{eV}$, $V_{dd\sigma} = -0.20\text{eV}$, (b) 50% $V_{dd\pi} = -0.25\text{eV}$, $V_{dd\delta} = -0.375\text{eV}$, $V_{dd\sigma} = -0.125\text{eV}$, and (c) 80% $V_{dd\pi} = -0.25\text{eV}$, $V_{dd\delta} = -0.45\text{eV}$, $V_{dd\sigma} = -0.05\text{eV}$. The resulting Chern number is presented in Fig. 11. Next, we increase the anisotropy to 80%, the resulting Chern profile significantly changes and shows no more clear plateaus at $C = \pm 5$. This result indicates that the predicted large Chern number is robust even against relatively strong anisotropy in the Slater-Koster integrals; the large Chern number is not limited to the isotropic limit of hopping integrals in the model, but persists even in the presence strong anisotropy in the Slater-Koster integrals. The predicted large Chern number $C = \pm 5$ can thus occur in real materials, where the Slater-Koster integrals normally very anisotropic, as long as the nontrivial gaps remain. The only downside of anisotropic Slater-Koster integrals is that such nontrivial gaps become much

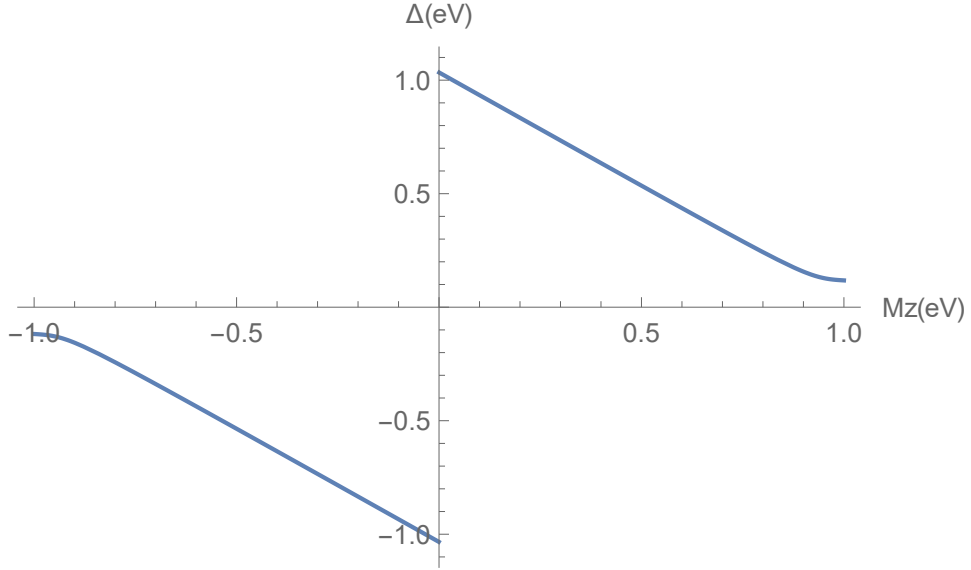


FIG. 7. The dependence of the gap Δ on M_z . Parameters used are $t = -0.25\text{eV}$, $M_s = 1.0\text{eV}$ where $M_z = M_s \cos \theta$.

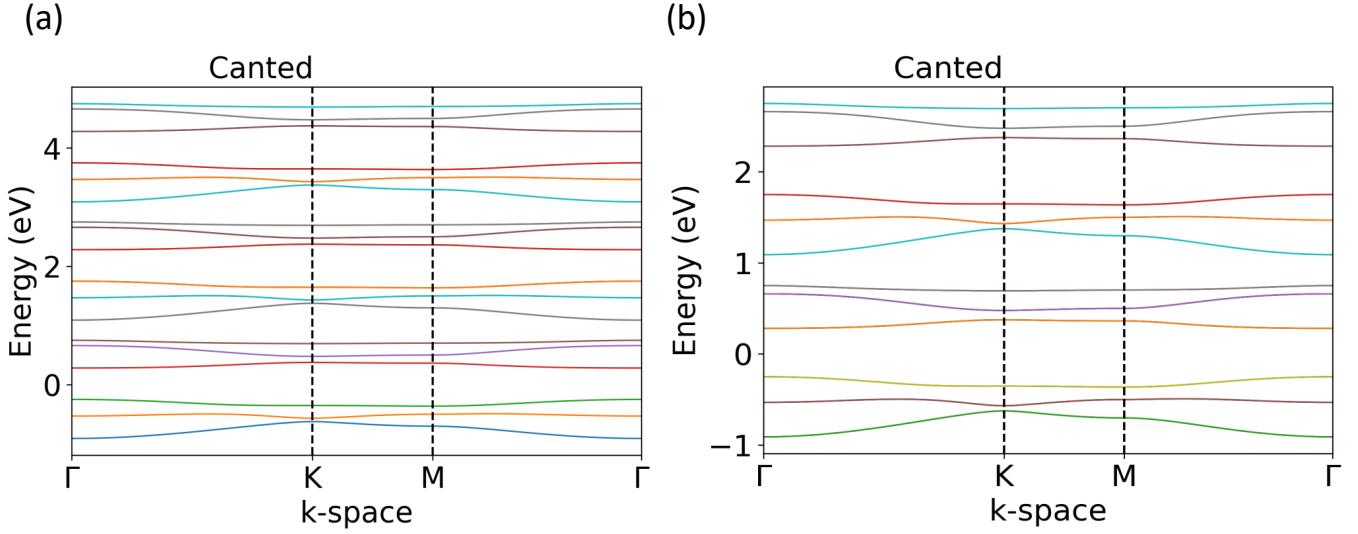


FIG. 8. Electronic band structures for non-coplanar (canted) non-collinear spin orders at $\theta = 53^\circ$ and $M_s = 1.0\text{eV}$ with isotropic Slater-Koster integrals $V_{dd\sigma} = V_{dd\delta} = V_{dd\pi} = -0.25\text{eV}$ and different onsite energies: (a) $E_{z^2} = 0.0\text{eV}$, $E_{xz,yz} = 2.0\text{eV}$, and $E_{xy,x^2-y^2} = 4.0\text{eV}$ and (b) $E_{z^2} = 0.0\text{eV}$, $E_{xz,yz} = 2.0\text{eV}$, and $E_{xy,x^2-y^2} = 0.0\text{eV}$.

narrower, as attested in Fig. 12, making it harder to fine tune the Fermi energy (filling factor or electron density) to realize the coveted large Chern quantum anomalous Hall effect.

C. Dependence of Chern Number C on Canting Angle

The Chern number turns out to be robust with respect to the canting angle. The profiles of Chern number vs. Fermi energy for a set of three canting angles (small $\Theta \approx 0$, moderate $\Theta \approx \pi/4$, and large $\Theta \approx \pi/2$) are shown in Fig. IVC. In all three cases, the Chern peaks with $|C| = 5$ exist. This finding is easy to explain. As shown in¹², in an electron model on kagome lattice with flux Φ in triangle, the resulting Chern number characterizing quantum anomalous Hall effect only depends on the sign of the flux; $C = \text{sgn}[\sin(\Phi)]$. As such, the actual value of the flux (related to the canting angle Θ) as given by Eq.(2) in the main text, does not really matter; as long as it is neither zero nor π , the Chern number (from each of d orbital) would be nonzero $C = \pm 1$.

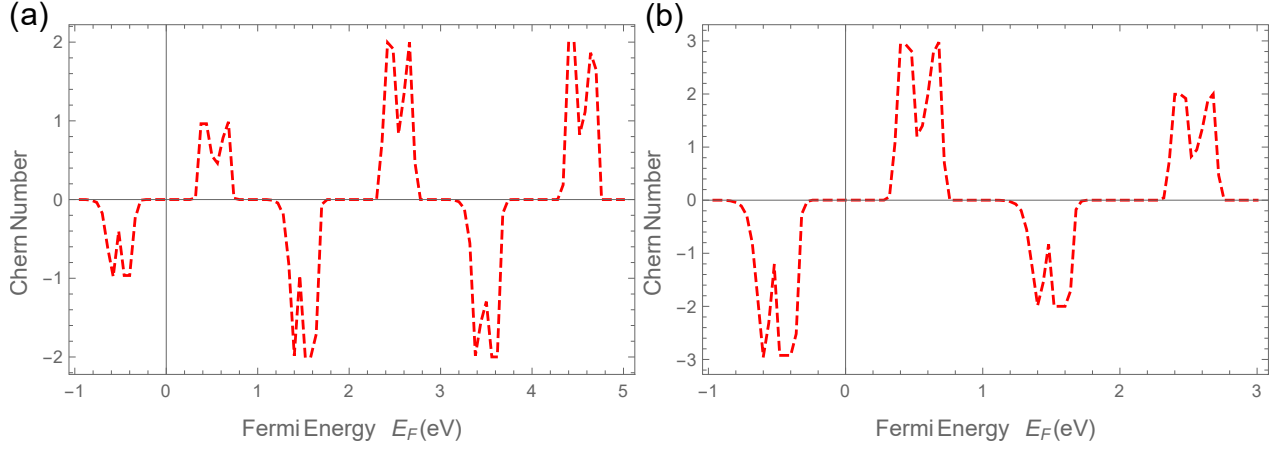


FIG. 9. The dependence of the Chern number C on the Fermi energy E_F (eV) at $T = 0.0001\text{eV} (= 1.1\text{Kelvin})$ for kagome d -electron system with 120° canted (non-coplanar) antiferromagnetic order, with well separated onsite energies (a) $E_1 = 0.0\text{eV}$, $E_2 = 2.0\text{eV}$, and $E_3 = 4.0\text{eV}$, giving a set of plateaus with $C = \pm 1, \pm 2$. A different set of parameters (b) $E_1 = 0.0\text{eV}$, $E_2 = 2.0\text{eV}$, and $E_3 = 0.0\text{eV}$ gives a series of Chern numbers $C = \pm 3, \pm 2$.

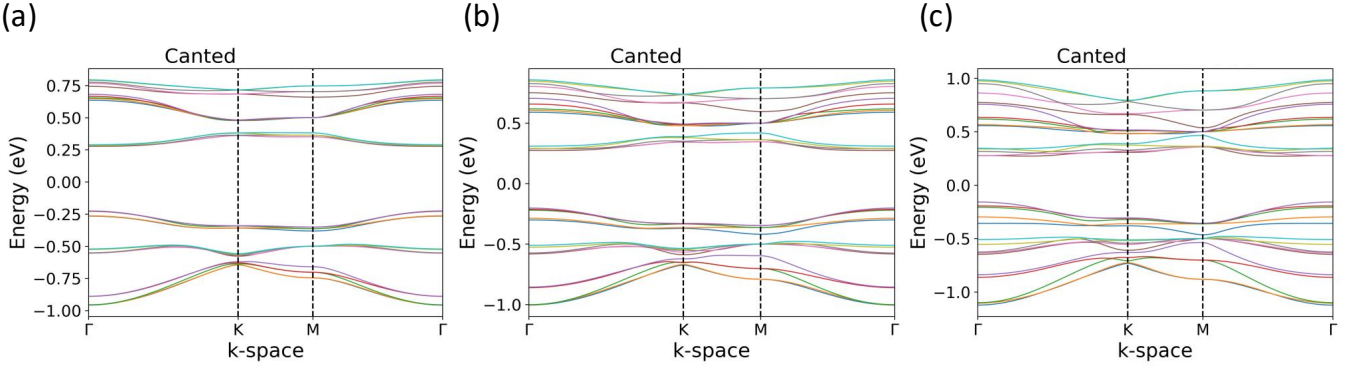


FIG. 10. Electronic band structures for non-coplanar (canted) non-collinear spin orders and anisotropic Slater-Koster integrals by: (a) 20%; $V_{dd\pi} = -0.25\text{eV}$, $V_{dd\delta} = -0.30\text{eV}$, $V_{dd\sigma} = -0.20\text{eV}$, (b) 50% $V_{dd\pi} = -0.25\text{eV}$, $V_{dd\delta} = -0.375\text{eV}$, $V_{dd\sigma} = -0.125\text{eV}$, and (c) 80% $V_{dd\pi} = -0.25\text{eV}$, $V_{dd\delta} = -0.45\text{eV}$, $V_{dd\sigma} = -0.05\text{eV}$, all of which without SOC and with equal onsite energies set to zero. In (a), all the four nontrivial gaps survive, while in (b) and (c), only two of the four of them survive; the other two get overlapped by bands.

¹Qi, X. L., Wu, Y.-S., and Zhang, S.-C., Topological quantization of the spin Hall effect in two-dimensional paramagnetic semiconductors, Phys. Rev. B 74, 085308 (2006).

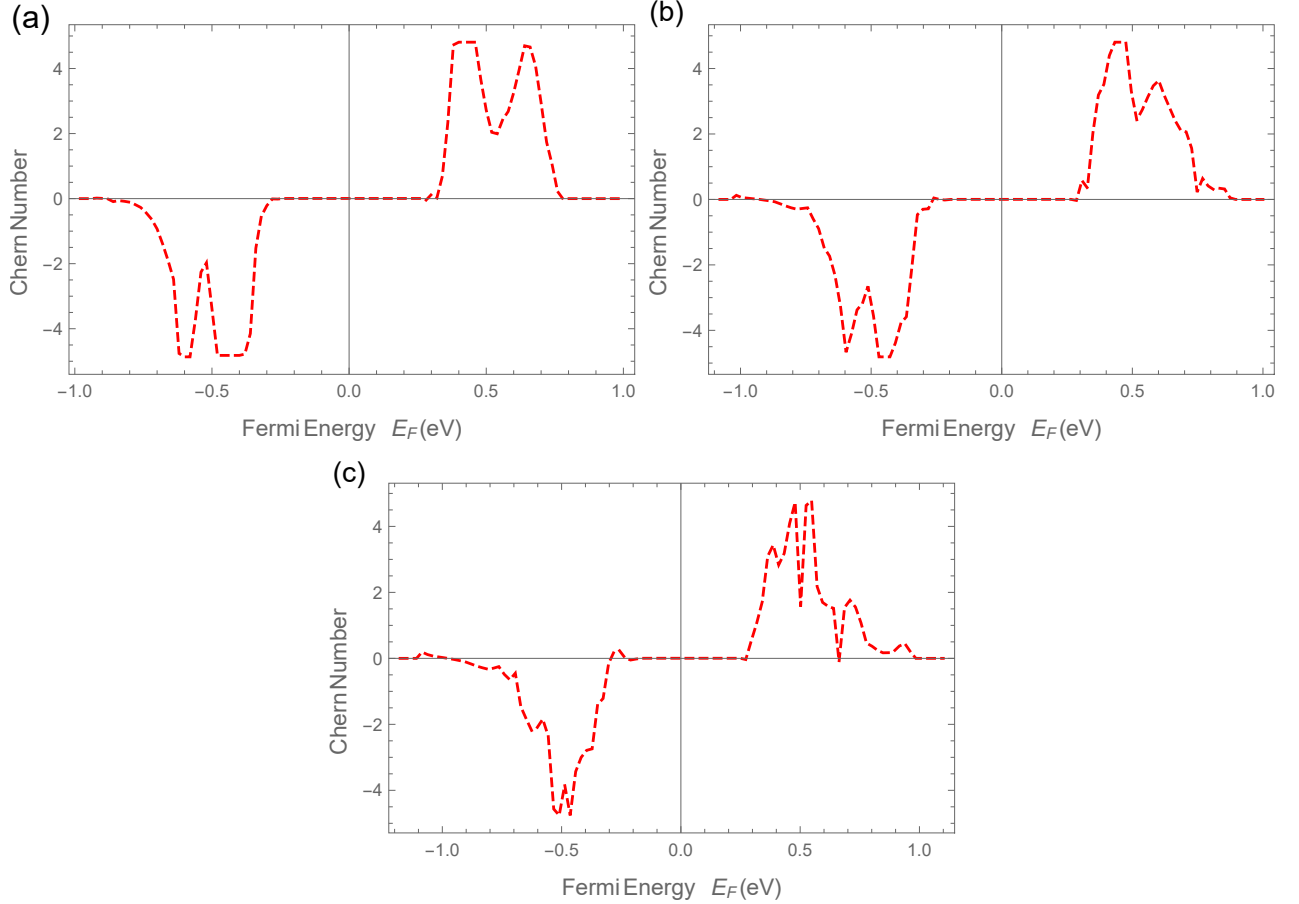


FIG. 11. The dependence of the Chern number C on the Fermi energy E_F (eV) at $T = 0.0001\text{eV} (= 1.1\text{Kelvin})$ for kagome d -electron system with 120° canted (non-coplanar) antiferromagnetic order, with anisotropic Slater-Koster integrals (top, 20% anisotropy), still giving the same set of record-breaking value of large Chern number $C = \pm 5$. Stronger anisotropy by 50% (middle) and 80% (bottom) reconfigures the Chern number profile entirely with still visible peaks at $C = \pm 5$, despite much narrower energy bandwidth.

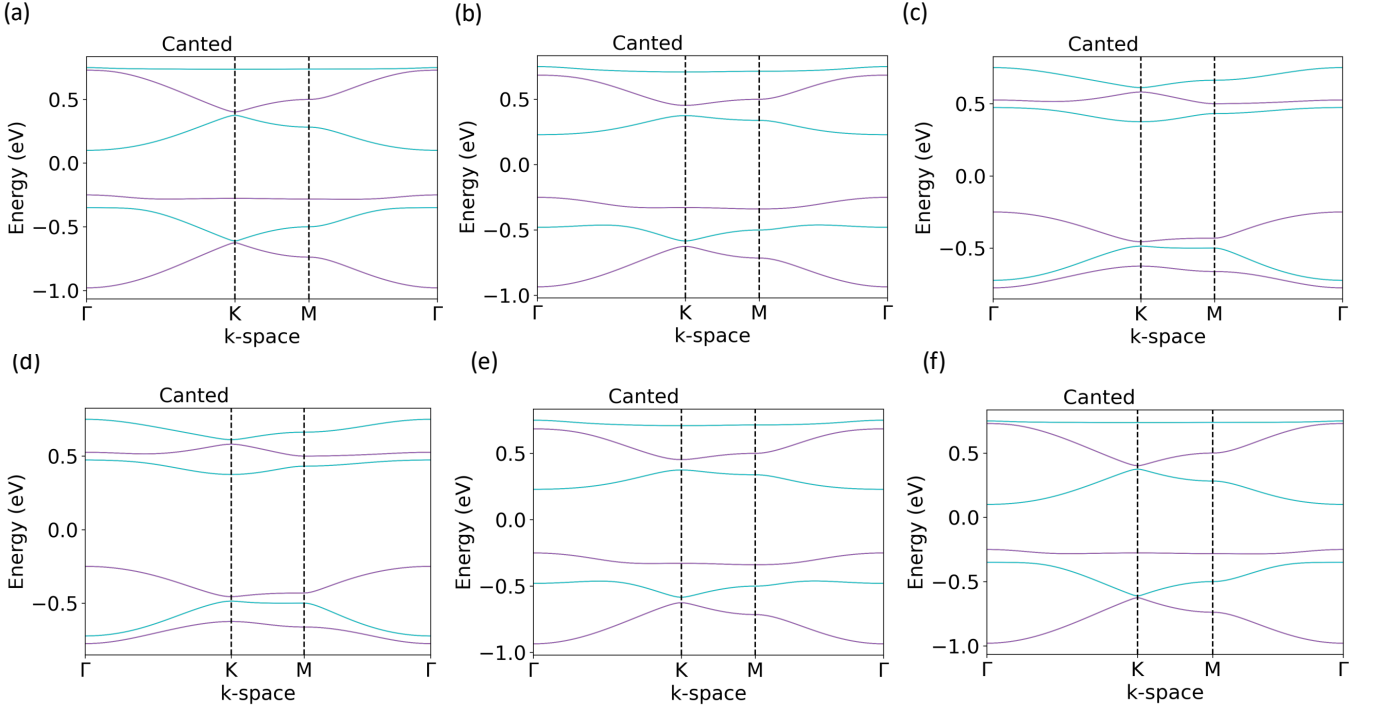


FIG. 12. Electronic band structures for non-coplanar (canted) non-collinear spin orders and isotropic Slater-Koster integrals V , but with different canting angle: (a) $\theta = 15^\circ$, (b) $\theta = 45^\circ$, (c) $\theta = 85^\circ$, (d) $\theta = 95^\circ$, (e) $\theta = 135^\circ$, and (f) $\theta = 165^\circ$, all of which without SOC and with equal onsite energies set to zero. In (a), all the four nontrivial gaps survive, while in (b) and (c), only two of the four of them survive; the other two get overlapped by bands.

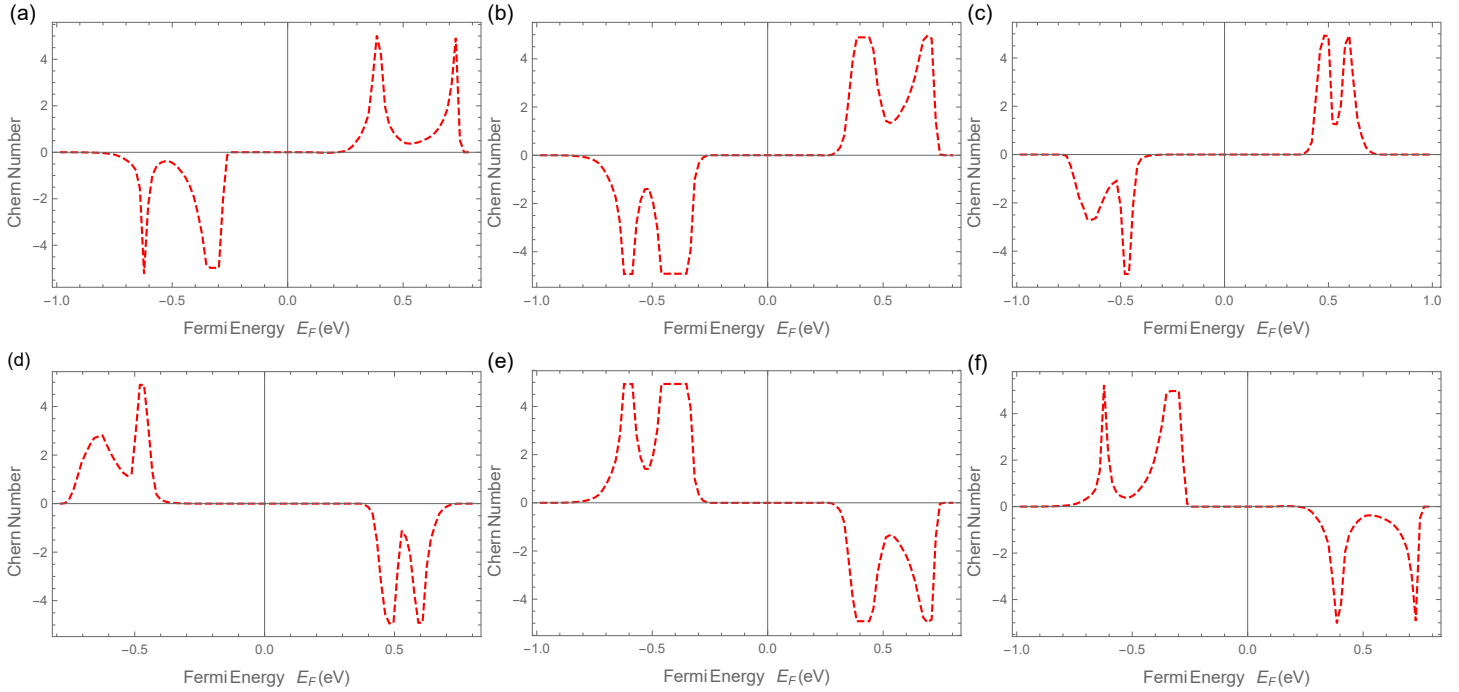


FIG. 13. The dependence of the Chern number C on the Fermi energy E_F (eV) at $T = 0.0001\text{eV} (= 1.1\text{Kelvin})$ for kagome d -electron system with 120° canted (non-coplanar) antiferromagnetic order, on the canting angle with (a) $\theta = 15^\circ$, (b) $\theta = 45^\circ$, (c) $\theta = 85^\circ$, (d) $\theta = 95^\circ$, (e) $\theta = 135^\circ$, and (f) $\theta = 165^\circ$ (measured from z axis), while $M_s = \sqrt{M_x^2 + M_y^2 + M_z^2} = 1.0\text{eV}$ is fixed, still giving the same set of record-breaking value of large Chern number $C = \pm 5$.